Modeling of high-fluence irradiation of amorphous Si and crystalline Al by linearly focused Ar ions

A. Lopez-Cazalilla,* A. Ilinov, and K. Nordlund
Department of Physics, P. O. Box 43, FIN-00014 University of Helsinki, Finland

F. Djurabekova
Department of Physics, P. O. Box 43, FIN-00014 University of Helsinki, Finland
Helsinki Institute of Physics, Helsinki, Finland and
National Research Nuclear University MEPHI, Kashirskoe avenue, 31, Russia, Moscow

(Dated: November 27, 2018)

Long time ion irradiation of surfaces under tilted incidence causes formation of regular nanostructures known as surface ripples. The nature of mechanisms leading to ripples is still not clear, this is why computational methods can shed the light on such a complex phenomenon and help to understand which surface processes are mainly responsible for it. In this work, we analyse the surface response of two materials, a semiconductor (silicon) and a metal (aluminium) under irradiation with the 250 eV and 1000 eV Ar ions focused at 70° from the normal to the surface. We simulate consecutive ion impacts by the means of molecular dynamics to investigate the effect on ripple formation. We find that the redistribution mechanism seems to be the main creator of ripples in amorphous materials, while the erosion mechanism is the leading origin for the pattern formation in crystalline metals.

I. INTRODUCTION

The nanopatterning effect caused by ion irradiation has been widely studied for different materials[1–3] and for various irradiation energies[4–7]. Depending on experimental parameters, such as ion energy, temperature of the system, type of ions and material of a substrate, and irradiation angle, a range of different periodic surface structures can appear, e.g. well-ordered dots or nanoripples[8,9].

The role of atomic redistribution during ion irradiation has been discussed in, for example, Refs. 10 and 11 as a competitive, or even dominating effect for the process of nanoripple formation as compared to the the erosion effect. Using the crater function formalism[12], one can estimate quantitatively the contribution of each effect. For instance in Ref. 13, we performed sequential irradiation of a-Si for low energies ($E_0 \geq 30$ eV); in this energy regime, intensive sputtering cannot be expected and thus, the erosive mechanism of ripple formation can be neglected. Nevertheless, we observed that small displacements in each ion impact cumulatively caused formation of the groove and the ripple on the surface. If the ion energy is increased, the erosive mechanism in the surface pattern formation becomes more prominent. Then the redistributive mechanism is not sufficient to describe the process of the pattern formation as it is in Ref. 13. On the other hand, the crater function formalism[12] is very handy to predict the pattern formation with both erosive and redistributive mechanisms present as we did in 10 and 11. However, the assumption of a flat surface (increase of surface curvature will affect the linearity of the main equation in the theory) and the basic parameters obtained only for single ion impact simulations, limit the applicability of this formalism for more realistic irradiation conditions.

On the other hand, the role of erosion has been discussed for many years[14–16] and been used to predict the pattern formation[17] and propagation velocity of the created structures[18].

The combination of both erosion and redistribution during the sample irradiation seems to lead to the formation of the final surface effect. Each contribution takes more or less importance in function of different parameters like energy or irradiation angle. Moreover, the simulation method may lead to different conclusions about the reason of the formation. Specifically molecular dynamics considers small displacements that are determinant for the ripple formation[10] at low and medium energies, which binary collision approximation[19] does not consider.

In the current paper, we apply the same methodology as described in Ref. 13 to allow for realistic evolution of the surface curvature, but for higher ion energy range. In this condition of ion irradiation, the sputtering becomes non-negligible, so we can analyze concurrently the surface modification due to both effects. Moreover, to obtain the deeper understanding of the effect of the redistributive mechanism on pattern formation in the regime of dynamic modification of surface curvature, we simulate irradiation of a-Si and monocrystalline aluminium (c-Al) materials.

Since many defects formed in crystal structures during the development of a cascade are rapidly annealed after the cascade has been stopped[20], the strain field formed by the remaining defects is expected to be much smaller compared to that formed by many atomic displacements during the cascades in amorphous materials. These remain in the structure also after the cascade. The differences between both materials suggest that the nature of the formation of ordered structures in the surface is different, since experimentally it has been observed in polycrystalline[21–24] and monocrystalline metals[25], and the only available explanation for the formation of the

structures is the erosion. In addition, the fluence needed to induce ripples in Al films is about the same order of magnitude[23] (10^{17} ions/cm^2) compared to the same effect in Si.

The paper is organized as follows: in Section II we explain how we proceed to reproduce the surface modification. We continue with Section III, where we observe and discuss the results obtaining, focusing in the main differences between both materials regarding the redistributive and erosive mechanisms. Finally in Section IV we point out the main outcomes of this work.

II. METHODS

We used PARCAS MD code[26,27] to perform the ion irradiation simulation of a-Si and c-Al materials with 10000 and 4000 Ar^+ ions of 250 eV and 1 keV energies, respectively. The irradiation was performed at 70° off-normal, which is one of the angles at which the pattern formation in Si is the most likely to be observed[10]. Moreover, it is well established that sputtering yields increase when the incident angle increases from normal incidence (perpendicular impact), having a maximum around 70° off-normal[28,29]. We have also simulated most cases with 80°, 85° and 88° tilt of incidence. The sequential irradiation of the cell was performed within a stripe on the surface parallel to the y axis and of 1.6 nm in the width (in x direction) to imitate a linearly focused ion beam similarly as we did in Ref. 13. Such an approach was adopted to reduce the required amount of sequential simulations before a significant response of the surface can be observed. Periodic boundary conditions are applied in the x and y directions. The schematics of the simulation setup is shown in FIG. 1. After every impact, the cell was shifted randomly along the periodic y direction to enable the randomness of the entrance point of the ion, while the main direction of the incoming ion was always directed perpendicular to the y axis. The x coordinate was selected randomly within the specified range. At the end of every impact, those particles which are sputtered away (above 2.5 nm from the initial surface) and those that reach the fixed layer are removed before the next impact. The reason of removing the atoms which penetrates the fixed layer is because we wanted to leave the layer intact in order to prevent the system motion. Two similar simulations were run in order to observe how the removal of those atoms influenced the shape of the surface, one removing the atoms which penetrates the fixed layer and the other keeping them for the next simulation. Up to 4000 Ar^+-250 eV impacts were simulated at normal incidence (where most of the momentum is introduced in the z-direction) on the a-Si cell. The result indicated that the surface modification in both cases are similar.

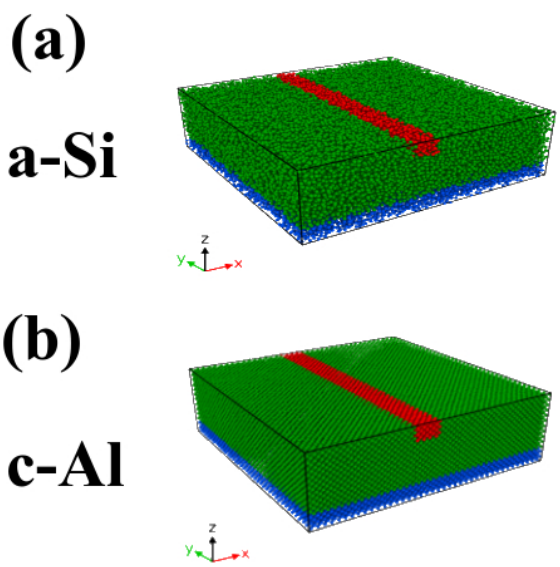

FIG. 1: Initial simulation cells: (a) a-Si cell and (b) c-Al cell. Red: effective irradiation region. Blue: Fixed layer

Since it is important to analyze all small displacement that survive in the structure after the cascade, we relaxed the system carefully before the irradiation simulations. For the a-Si case, we used the same cell as in Ref. 13, where the relaxation process was explained in detail along with the simulation parameters. The c-Al target was prepared as follows. A periodic FCC Al structure was created at 0 K and then heated up to 300 K during 10 ps while maintaining the zero pressure. After this initial step, the surface in z direction was opened, and the system was simulated for another 10 ps in order to relax the open surface prior to irradiations. The relaxation process of c-Al target is presented in FIG. 2.

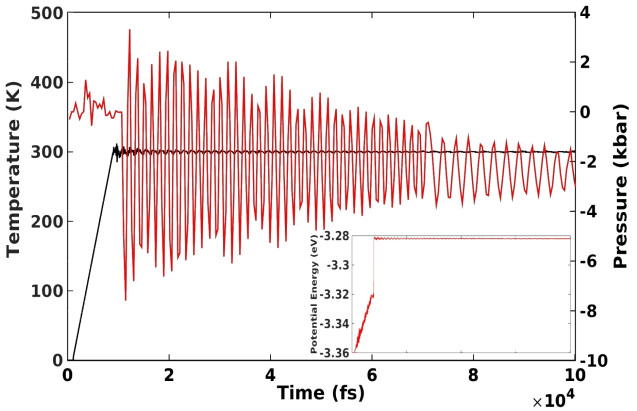

FIG. 2: Relaxation of c-Al structure. Inset: Evolution of the potential energy as function the time. Main graph: Evolution of the temperature (black) and pressure (red).

As we can observe from the FIG. 2, the system reached the final temperature of 300 K, and there was sufficient

time to allow for stabilization of the potential energy and the pressure.

The final size of the cell in this case is 16.20 × 16.20 × 5.27 nm^3. A fixed layer of 1 nm at the bottom prevented the system displacement during the simulations. PARCAS MD[26,27] code differentiates between irradiation and non-irradiation processes in the way the time step is chosen[30], i.e. shorter time steps during irradiation prevent energetic recoils to move a considerable distance in a single time step. The time step also depends on the mass of the atoms involved in the simulation. The time steps for the irradiation were 0.29 fs at 250 eV Ar^+ and 0.14 fs for the 1000 eV Ar^+, and in the temperature rescaling process were 2.16 fs and 1.59 fs respectively for Si and Al. Further details on the time steps are available in Ref. 30. A thermal bath of 0.8 nm thickness at all sides of the cell except the top prevented the overheating of the cell during the irradiation simulations during first 21 ps, and then, for another 8 ps the temperature in the simulation cell was linearly scaled to 300 K again before the next impact run.

The interaction between the Al particles was described by the Embedded-atom method (EAM) potential for Al[31] joined by the repulsive ZBL[32] potential at short distances; the combined potential was fine-tuned to give correct values of the threshold displacement energy [33]. The Ar-Al interaction was described using the pure repulsive ZBL potential[32]. Since the Ar atoms are preserved between the different impacts, the Ar-Ar interaction was considered using a potential with a high energy repulsive part from DFT DMol calculations [34] for small distances joined smoothly to the LJ equilibrium part [35].

In the following, we will distinguish two contributions in the effect of surface modification: erosive (sputtering), which includes atoms leaving the surface as a consequence of atomic collisions, and redistributive (displacement), which includes atoms relocating within the surface since their energy is insufficient to leave the surface. The latter will be analyzed as a total displacement in the system calculated as

$$\delta_w = \sum_{i=1}^{N_{displaced}} (w^i_{final} - w^i_{initial}), \qquad (1)$$

where δ_w represents the sum of the atomic displacement in the three direction (the three components of the total displacement vector) of the cell $w = \{x, y, z\}$ from the initial configuration.

III. RESULTS & DISCUSSION

A. Irradiation of a-Si under different incident angles

1. *Change in a-Si configuration*

The profiles of the a-Si cell irradiated with the 250 eV Ar ions at different incident angles and two fluences of 2000 and 10000 ions are presented in FIG. 3.

As we can see in FIG. 3, irradiation at 70° causes the strongest change in the surface profile. This also leads to the fact that during the ion bombardment, the incident angle also changes locally due to the changes in surface curvature, provoking the formation of a ridge growing upwards, and also pushing the material toward the positive x direction. Irradiation at 80° causes lesser surface modification, since θ is closer to grazing incidence. In this case, the created groove is shallower, and the ridge is displaced faster along the surface due to a larger momentum transferred by ions to the surface atoms in the x direction. At 85°, the Ar^+ ions modify the surface even less, showing formation of a groove only at the end of 10000 ion impacts. Finally, the 88° incident angle does not cause any surface modification, the surface profile stays flat, and the main effect, which is observed in this case is a small expansion (swelling) towards the z direction.

In FIG. 4, we present similar results for 1000 eV irradiation of a-Si,

From FIG. 4 it is evident that the erosion is higher compared to the results of 250 eV irradiation. Unfortunately, we were not able to produce results for the same fluence as the lower energy irradiation simulations, as the simulated cell was not thick enough to continue simulations after 4000 impacts. After this, the erosion process during the irradiation at 70° of incidence started removing the material close to the fixed layer of the cell, which may lead to simulation artefacts.

Comparing the surface profiles after 2000 consecutive impacts for both 250 eV and 1000 eV Ar^+ ion energies, we see that the observed effects for corresponding incidence angles are similar, but clearly larger in magnitude for the higher energy. However, we notice an important difference: The ridge formed at 70° irradiation with 1000 eV ions has a different shape compared to the similar case of 250 eV ion irradiation. Instead of a "piled-up" shape, the ridge is flatter and straighter. The reason is that secondary and higher order recoils that are formed in the 1000 eV cascades and have enough energy to continue displacement process further from the initial impact, which will be discussed below in more details.

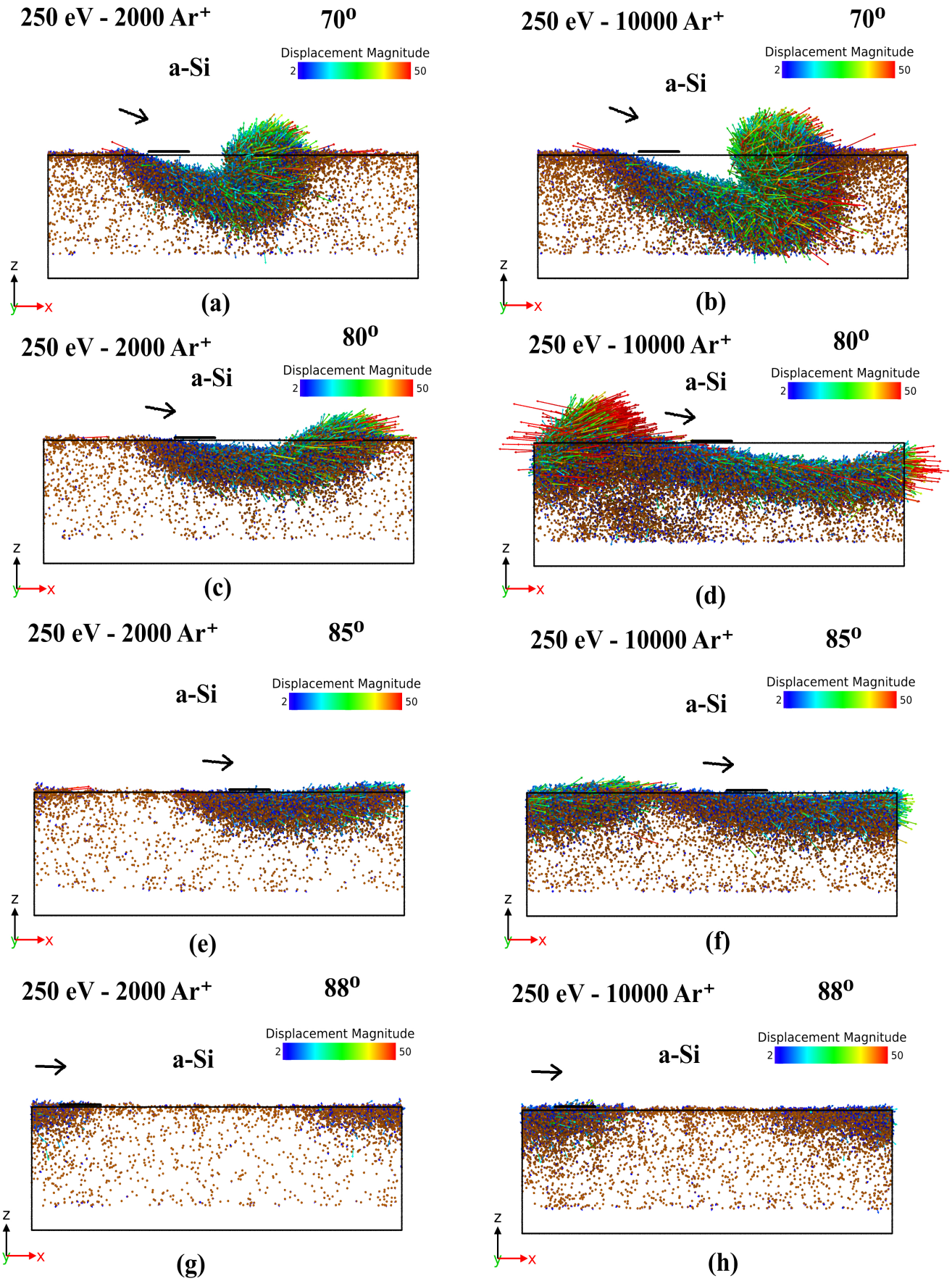

FIG. 3: a-Si cell under 250 eV Ar^+ after (a) 2k impacts and (b) 10k impacts at 70°; after (c) 2k impacts and (d) 10k impacts at 80°; after (e) 2k impacts and (f) 10k impacts at 85°; and after (g) 2k impacts and (h) 10k impacts at 88°. Only displacements greater than 2 Å are presented; the displacement vectors are scaled by a factor of 0.3 for a better visualization. The initial impact region is marked in black.

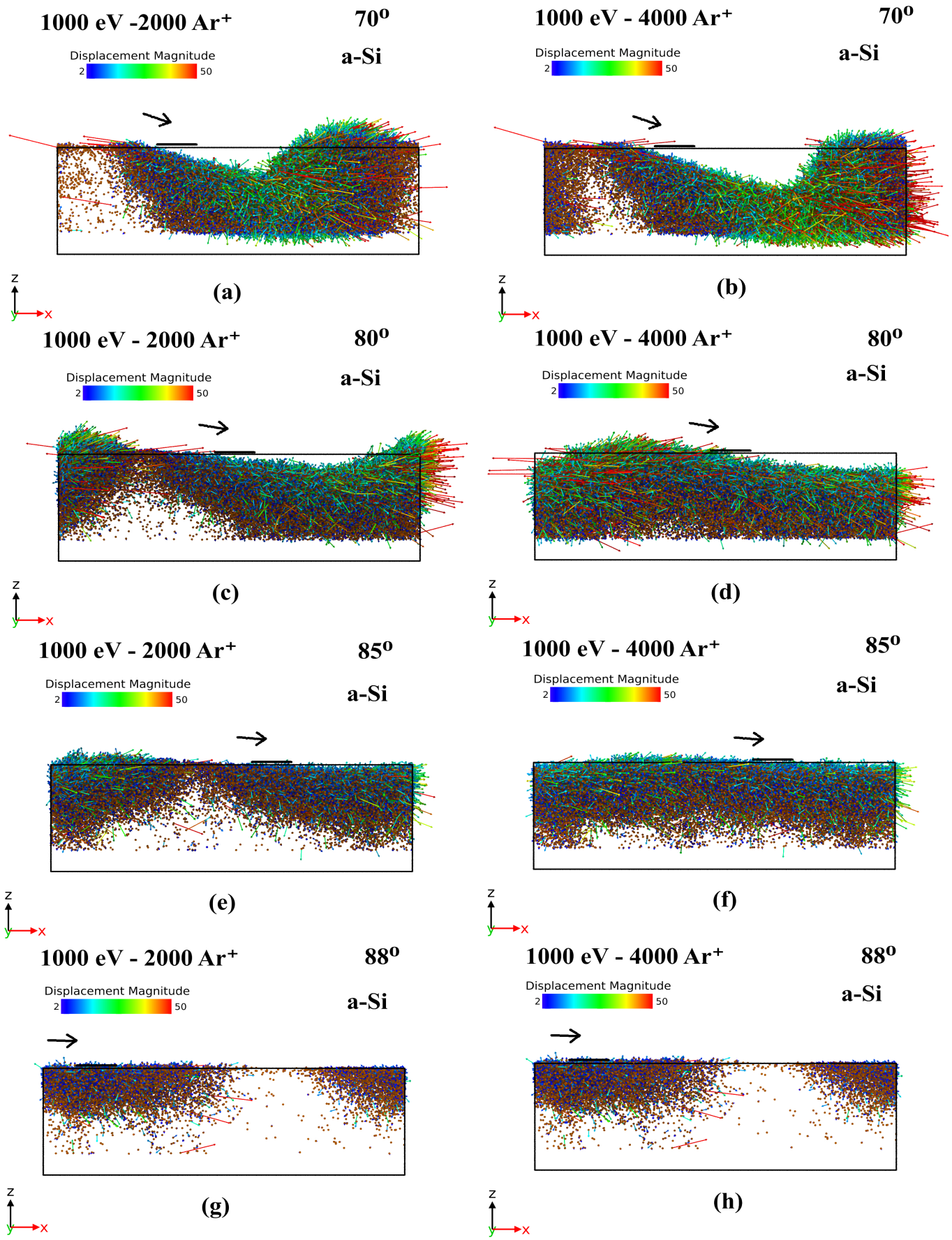

FIG. 4: a-Si cell under 1000 eV Ar^+ after (a) 2k impacts and (b) 4k impacts at 70°; after (c) 2k impacts and (d) 4k impacts at 80°; after (e) 2k impacts and (f) 4k impacts at 85°; and after (g) 2k impacts and (h) 4k impacts at 88°. Only displacements greater than 2 Å are presented and the displacement vectors are scaled by a factor of 0.3 for a better visualization. The initial impact region is marked in black.

2. *Sputtering-Displacement analysis for a-Si*

Based in the evolution of the a-Si cell during the irradiation, we analyse the data extracted regarding the erosive and redistributive mechanisms in FIG. 5.

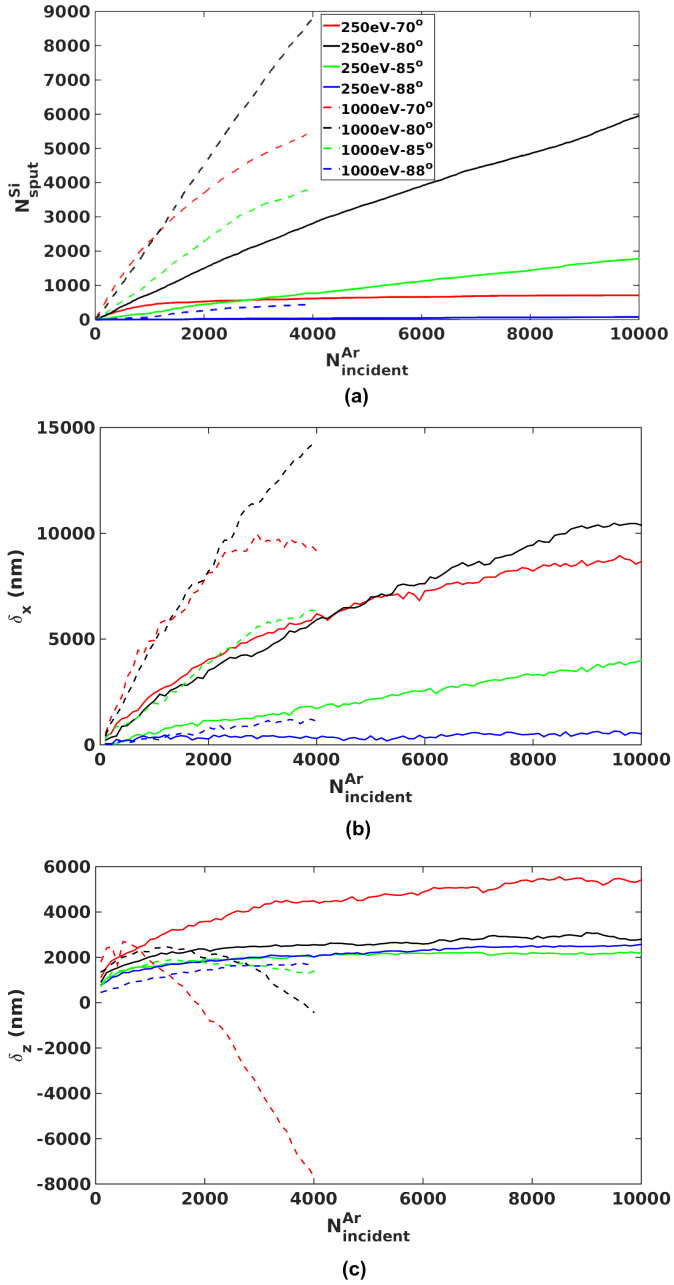

FIG. 5: Results for a-Si: (a) total sputtered atoms, (b) total displacement in x direction from the initial structure and (c) total displacement in z direction from the initial structure.

FIG. 5a shows the evolution of the number of sputtered atoms for both 250 eV and 1000 eV irradiation energies as a function of subsequent incoming ion. The same functions for the total dislacements in x and z directions calculated according to EQ. 1 are shown in FIGs. 5b and 5c. The displacement in the y direction is not presented, because the projection of the ion beam direction to y is 0, and due to symmetry considerations it fluctuates around zero and is not determinant for this study.

We see in FIG. 5a that erosion is a monotonically increasing function of the number of incoming ions, which means that the sputtering yield does not change or only slightly changes from impact to impact, although we observed some surface modifications in almost all cases. The intensity of the erosion is also increasing with decrease of the incident angle (closer to the normal one) for both energies. For the 80° incidence, we see that the amount of sputtered atoms is the greatest for the ions of both energies, and it grows monotonically without showing any tendency for saturation. At 85°, the erosion is less intense for the 250 eV ions than for the 1000 eV case, however, in the former case it is monotonically increasing, while in the latter case, the increase is slower after more than 2500 impacts. This can be explained by the behavior of the sputtered atoms. Since the energies of the sputtered atoms are lower at 250 eV ion impact, they can redeposit back to the surface easier than those sputtered by 1000 eV ions. However, the surface roughening after many impacts increases the sticking probability of the atoms sputtered even by the 1000 eV ions, contributing less to the total sputtering yield. We do not expect a full saturation of the sputtering yield until a very significant modification of the surface, which would be able to block the sputtering process completely. In the case of 88°, the ions with 250 eV incident energy are not able to sputter many atoms. They can only cause some redistribution of atoms on the surface, which grows very insignificantly above the original level, see FIG. 3g and 3h. Thus the erosion in this case is almost negligible. The ions of the 1000 eV energy, however, are still able to initiate some erosion, which mostly causes just general surface roughening, but not a formation of a groove and a ridge.

Irradiation at 70° presents the exception of this general trend of an almost linear increase of the total number of sputtered atoms with the number of impacts for both energies. Since the erosion at this angle is the strongest, the incoming ions dig out the deep groove, which significantly changes the incident angle with respect to the newly formed surface. Now, some of the atoms are sputtered forward at the incidence angles larger than the original 70° (in fact, it is becoming closer to 80°, see FIG. 3 and 4b). These atoms have high probability to be captured by the ridge (redeposition effect), contributing to the growth of the structure. In the case of 1000 eV, this happens to a lesser extent, although the overall trend is very similar. This can also be seen in FIG. 5b. The evolution of the total displacement in the x direction, δ_x, goes over a peak after about 2500-3000 ion impacts for the 1000 eV ions.

Let us now look at the total displacements in the x and z directions: δ_x (FIG. 5b) and δ_z (FIG. 5c). In-

crease in δ_x towards positive values evidently indicates that the atoms are displaced in the direction of the ion beam. Overall a monotonic increase of δ_x shows some tendency for saturations for those cases, where the surface was modified the strongest: 70° and 80° (250 eV). Initially, the growth of δ_x for both angles is quite similar, slightly higher values for the 70° case may be explained by a deeper ion penetration and the created cascades. However, after the significant modification of the surface took place, many sputtered atoms redeposited in the positions with the smaller x coordinate compared to the initial position, contributing negatively to the total displacement at this angle. Hence the increase of δ_x slows down. The irradiation at 80° does not cause piling of the atoms and all the displacements happen mostly toward the positive x direction. This is why the growth of the ridge continues rapidly increasing after δ_x for 70° started to slow down, as can be observed in FIG. 5b, where a change of the slope can be noticed. Eventually, the number of sputtered atoms becomes significant and contributes notably to the value of δ_x, reducing the growth rate of this quantity as well. In the case of 1000 eV ions, similar tendencies are observed. However, we also see a drop in the δ_x value. Inspecting FIGs. 4a-4c we oberve a finite size effect, which is stronger in the case of the 70° irradiation. The large displacements overlap with the layers of fixed atoms, affecting the increase of the total displacement value δ_x. Both contributions, the surface modification (atom redeposition) and the finite-size of the simulation cell, reverse the growing tendency of the total displacement in the x direction.

Accumulation of the total displacement in the z direction, δ_z, is developing somewhat slower. It is understandable as the induced displacement in this direction is smaller for all investigated angles. It is interesting to note that although the direction of z total displacement component is in the negative z direction, we observe the positive growth of δ_z. This indicates that in total, the atoms are stronger displaced toward the surface. This feature is the most prominent for 70° irradiation, as we observe the formation of a ridge. The strong drop in δ_z toward the negative values indicates that the positively displaced atoms in the z direction tend to sputter rather than stay in the surface. Only those atoms, which received the momentum in towards the bulk contribute to δ_z. Intensive sputtering, which we observed for the 70° and 80° irradiations with the energy of 1000 eV, correspond exactly to the two δ_z with the sudden and abrupt change towards the negative values.

B. Simulation of irradiation of c-Al at 70° and 80° of incidence

1. *Change in c-Al configuration*

Now we analyze the results of the sequential linearly focused irradiation simulations of the c-Al target.

Although we aimed to perform the simulations for the same angles as for a-Si target, the results of 85° and 88° did not show any development of the surface structures as none of the atomic displacements produced during the cascades remained in the structure after the quenching phase of the cascade. Hence, we focus only on the two angles of incidence 70° and 80° for c-Al target. Results are shown in FIGs. 6 and 7. We see that the ions at both energies are able to produce a groove and a small ridge at 70°, similarly to what we observed for the 80° irradiation of a-Si, clearly due to redeposition of the atoms and erosion. In the case of 80°, the incoming ions experience more scattering and contribute much less to the damage formation in the surface, especially with the 250 eV incident energy. With increase of initial energy, the dynamics of the atomic collisions become more efficient, producing lasting displacements of atoms from their original positions. We see much stronger surface modifications in FIG. 7 as compared to the corresponding cases of FIG. 6 (note again that the higher energy case was simulated only until 4000 ion impacts).

2. *Sputtering-Displacement analysis for c-Al*

We analyse the erosive and redistributive mechanisms in FIG.8.

As can be seen in FIG. 8a, the only incidence angle which resulted in a considerable number of sputtered atoms for the 250 eV Ar ions was 70°. No irradiation simulation at larger incident angles caused either significant sputtering process, or significant total displacements: δ_x and δ_z, see FIG. 8b. The total number of sputtered atoms by the 250 eV ions at 80° was 18; out of these, some redeposited at the top of the surface. The total displacement due to relocation of these few atoms has blended within the displacements caused by regular thermal atomic vibrations.

Overall, the irradiation of the c-Al cell with the 1000 eV Ar ions resulted in more remarkable results. As we see in FIG. 8, the number of sputtered atoms at 70° of incidence is considerably larger than that for 80° irradiation, unlike the result for the a-Si cell. Here, we do not observe significant change of the surface curvature (see FIG. 5a), so the local incidence angle is not changing as much as it did at 70° incidence on the a-Si surface (see FIG. 4b).

FIG. 8b shows the evolution of the x component of the total displacement, δ_x. We see that δ_x is gradually growing for both ions with 250 eV energy at 70° of incidence and the 1000 eV ions at 80° of incidence. We observe rather abnormal behavior of δ_x for the 1000 eV ions at 70° of incidence, where δ_x grows first rapidly until approximately 2000 impacts, but then the growth slows down significantly. Although the sputtering is intense, the erosion shows close-to-linear behavior and would not be able to explain such a sharp transition in δ_x behavior. The finite-size effect due to choice of the simulation cell is

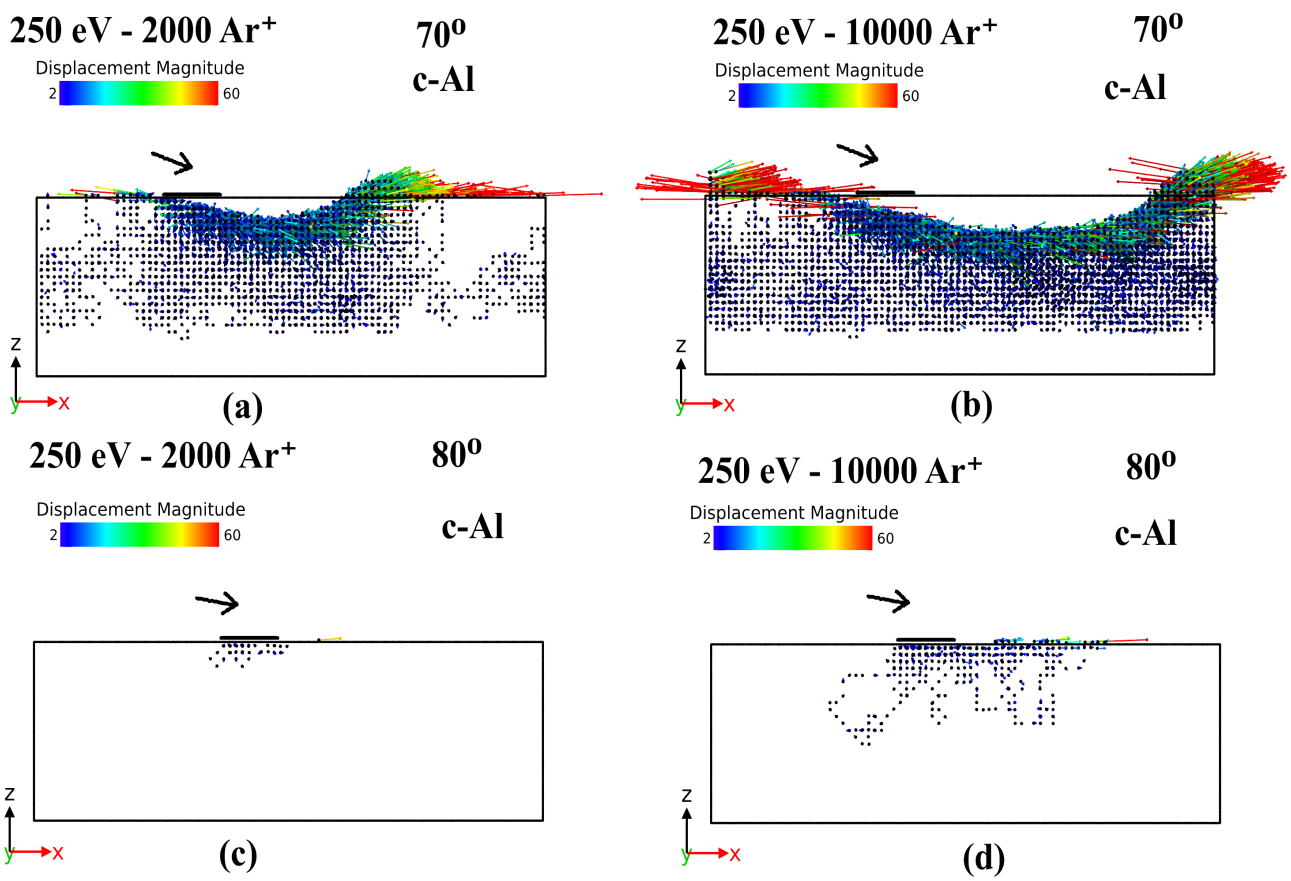

FIG. 6: c-Al cell after 250 eV Ar^+ (a) 2k impacts and (b) 10k impacts at 70°; and after (c) 2k impacts and (d) 10k impacts at 80°. Only those displacements greater than 2 Å are presented and the displacement vectors are scaled by a factor of 0.3 for a better visualization. The initial impact region is marked in black.

a more probable explanation, which is more prominent in the crystalline material compared to the amorphous one. Nevertheless, we report these results here as well, since the main conclusions of this work are not affected by this artifact. In the larger simulation cell, the behavior of δ_x is expected more monotonically growing similarly to what we observe for 80° incidence with 1000 eV ions and 70° incidence with 250 eV ions.

In FIG. 8c, we can see how the displacement in the z direction influences the formation of the groove. As we see, δ_z in the case of the 250 eV ions with the 70° incidence at first shows the increasing tendency towards more negative values. As the fluence increases, the trend reverses and already after the first few hundreds of ion impacts, δ_z grows towards the positive values. This indicates the formation of a ridge and overall tendency of displacements toward the surface. The 1000 eV ion irradiation at 70°, hammers the atoms inwards causing the gradual growth of δ_z towards the negative values. Intensive sputtering in this case, again reduces the positive component of δ_z, which would indicate the tendency for ridge formation. Instead, even if such positive component exists in these simulations, it is overtaken by the displacements deeper to the cell building up a well pronounced groove. However, combined together with the trend of the δ_x, we see that the groove is moved from the spot of the impact in the direction of the ion beam, which demonstrates the importance of the redistributive mechanism in the modification of the surface under long-term irradiation. The increase of the incidence angle to 80° reducing the negative tendency of the δ_z. At first it grows negative almost as fast as δ_z at 70°, but after a few hundreds of impacts, this tendency slows down, and we observe much slower increase of the negative value of δ_z. This indicates that the number of redeposited atoms at this point is increasing. Combining the evolution of both total displacement components, we conclude that the groove is more efficiently formed by the 1000 eV Ar ions at 70°, while the ridge can be expected at 70° by the ions with the energy of 250 eV and at 80° by the ions with energy of 1000 eV.

Since the crystal structure does not yield any changes in the surface landscape until it accumulates sufficient amount of defects, we analyze in FIG. 9 which kind of defects are formed in c-Al cell for the corresponding cases shown in FIG. 6 and 7. We have also analysed the num-

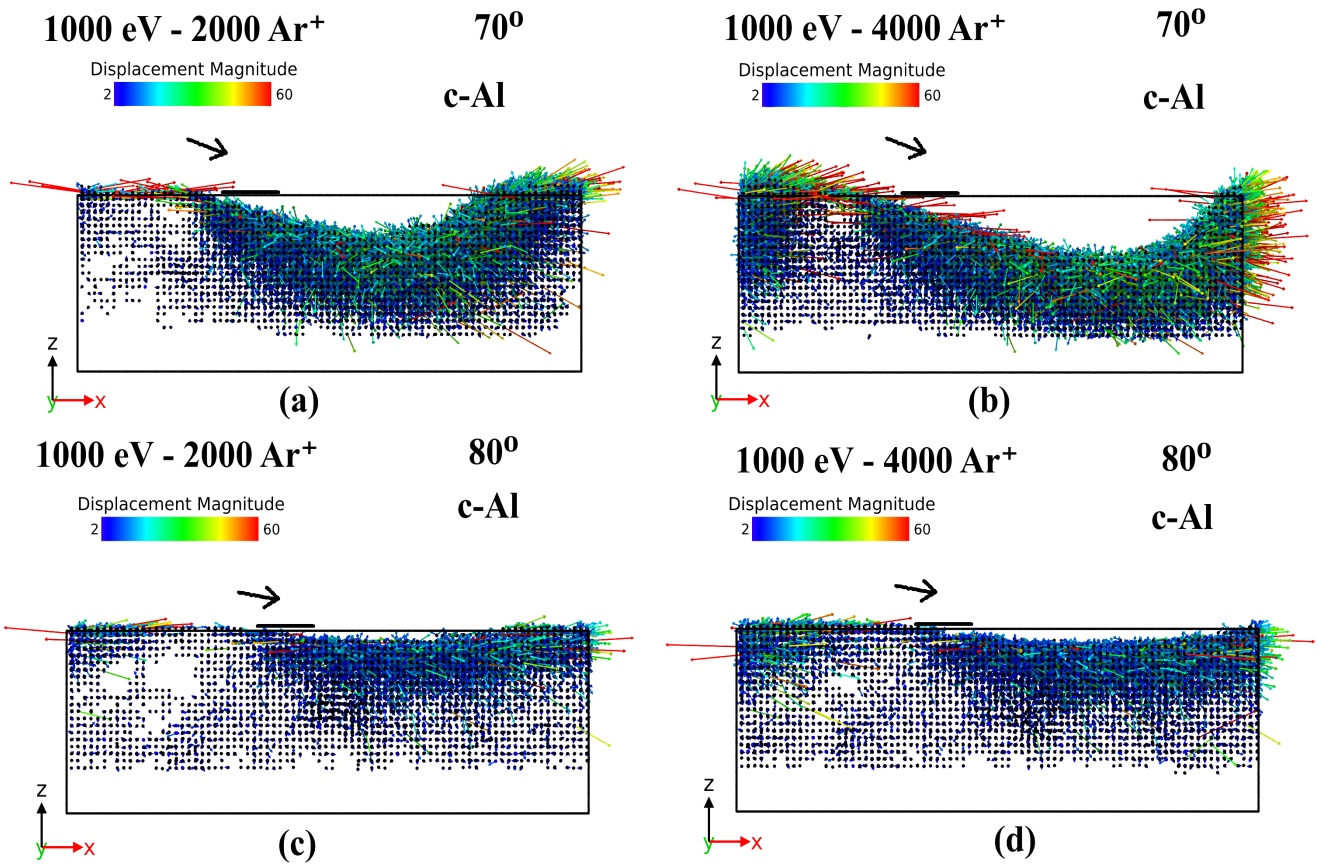

FIG. 7: c-Al cell after 1 keV Ar^+ (a) 2k impacts and (b) 4k impacts at 70°; and after (c) 2k impacts and (d) 4k impacts at 80°. Only those displacements greater than 2 Å are presented and the displacement vectors are scaled by a factor of 0.3 for a better visualization. The initial impact region is marked in black.

ber of coordination defects as the function of fluence. This analysis did not produce any appreciable dependence. In FIG. 9, we observe several important features specific for irradiation at different incidence angles and energies. In FIG. 9a and 9b, the irradiation creates defects on the surface as well as some isolated defect clusters beneath the surface along the path of the ion beam and high energy recoils promoting formation of a ridge next to the groove created by the sputtering. The 1000 eV Ar ions penetrate deeper in the bulk, creating defects not only in the surface, but also in the bulk. Formation of predominantly greater number of defects in the bulk observed for both incidence angles, 70° and 80° (FIG. 9f – 9h). However, these defects are evenly distributed in the structure, this is why the ridge is forming slower by the ions of this energy.

In the following we will compare the results obtained for these two materials, which are very close in the periodic table of elements, but different in the nature of bond formation and crystal structure. Previous comparisons of crystalline Si and Al have shown that due to the more open crystal structure in Si, atoms are displaced easier and are more likely to remain in a defective position than in the close-packed Al[27,33]. Other studies have shown that after Si is amorphized, a large number of atoms can also be permanently displaced by distances smaller than the interatomic separation[11,36]. Since pure metal never amorphize, such small displacements are not possible in Al. Moreover, as it was mentioned above, the surface response on irradiation effect is much slower in Al, since it requires formation and accumulation of permanent defects to cause any significant change in surface morphology, while much less energy is needed to displace an atom permanently in the amorphous environment.

C. Comparison of a-Si and c-Al

In this Section, we compare the irradiation effect at 70° since this incidence angle induced the strongest effect at all studied energies. In this analysis we also include the results of 30 eV irradiation. For the case of a-Si, the 30 eV results are adopted from Ref. 13.

At first, we analyze the distribution of the magnitudes of atomic displacements after 4000 Ar^+ impacts, where individual values are calculated as the magnitude of the

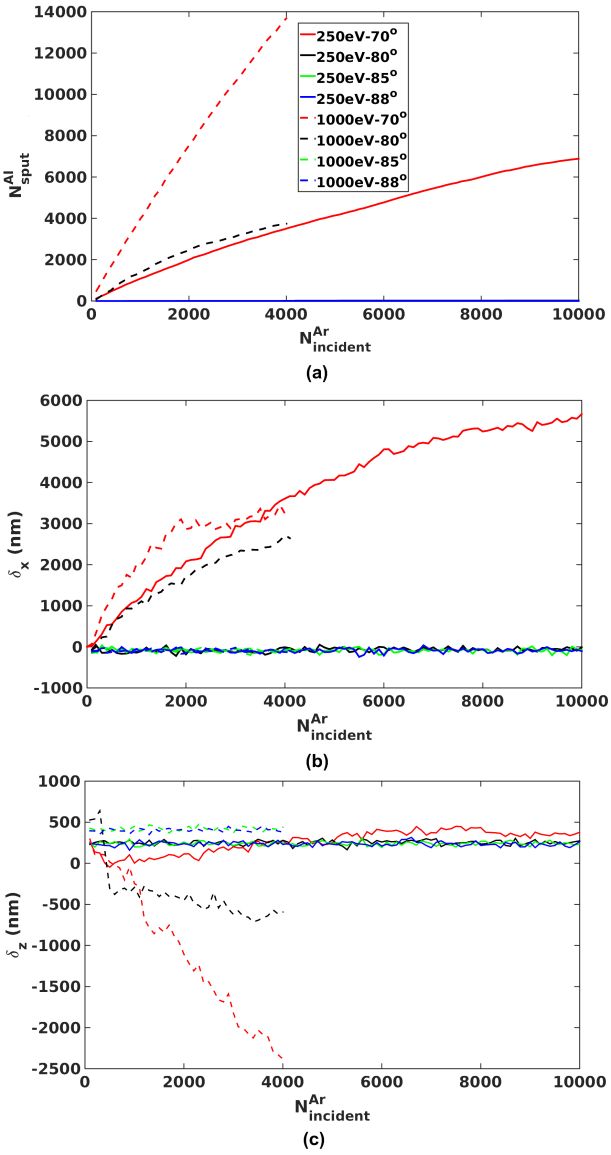

FIG. 8: Results for c-Al: (a) total sputtered atoms and (b) total displacement in x direction from the initial structure.

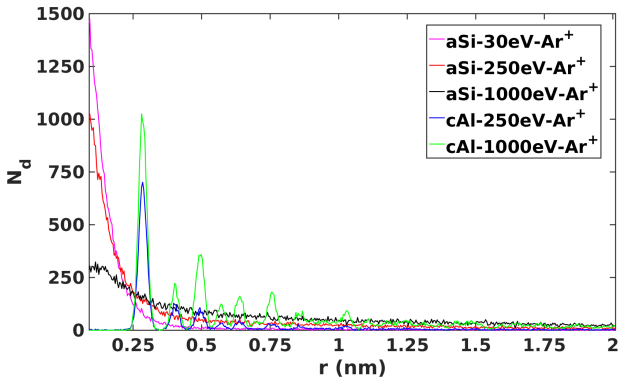

FIG. 10: Number of displacements as a function of the magnitude of those displacements after 4k impacts. Displacements below 0.1 nm are omitted (no appreciable displacement for 30 eV Ar^+ on c-Al). Data regarding 30 eV Ar^+ on a-Si is adapted from Ref. 13.

atomic total displacement vector ($r = \sqrt{\delta_x^2 + \delta_y^2 + \delta_z^2}$),

In FIG. 10, we clearly see the largest amount of displacements performed by atoms in all shown cases of irradiation of a-Si are under 0.25 nm. These contribute to formation of the groove as was found in Refs. 19 and 10. As expected, with the increase of the ion energy, the number of small displacement is decreasing, while the number of large displacement is increasing. It is also clear that the number of displacements of greater magnitude is more significant for the 1 keV case, which is reflected in a higher magnitude of the total displacement vector (FIG. 5). On the other hand, we cannot associate the groove formation with the small displacements in c-Al. As we see the number of displacement is an almost discrete function of the displacement magnitude. The maxima of these curves correspond to the sequential nearest neighbour (NN) distances. The atoms in the c-Al structure tend to be displaced and being captured more in positions of the 1st NN from their origin and less often in the more distant sites. Unlike the case of a-Si, in the crystalline Al structure the pattern formation is not due to small displacements, but due to the displacements defined by the FCC structure. We notice that for 250 eV the interstitials are trapped more often at the 2nd NN than in the 3rd NN, while in the 1000 eV cascades, the interstitials are trapped in 3NN positions more often. Overall, in all cases both the magnitude and number of those displacements are higher for 1000 eV impacts.

Now we take a closer look at the a-Si and c-Al structures after the 4000 Ar^+ impacts.

FIG. 11 shows clearly that the formation of a groove develops very similarly for both a-Si and c-Al structures at high energies, although the contribution of displacement of a specific type (see FIG. 10) can be different, which may result in the different shape of the groove and the ridge. For the case of 30 eV, the ion energy is insufficient to overcome the displacement threshold and this low-energy Ar irradiation does not induce any change in the surface morphology of the Al cell even after a high

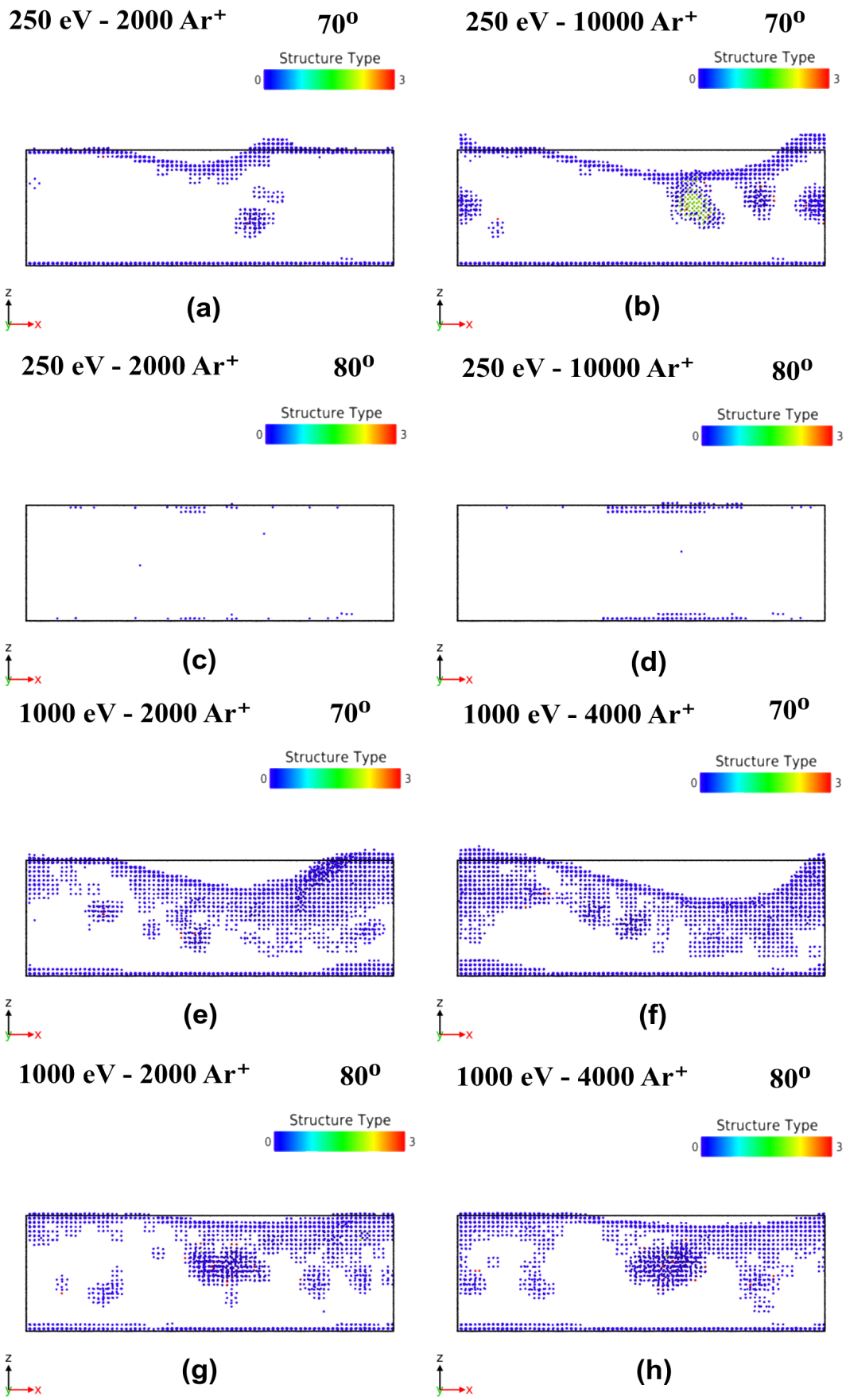

FIG. 9: Defect analysis of c-Al cell (shown in FIGS. 6 and 7) under 250 eV Ar^+ after (a) 2k impacts and (b) 10k impacts at 70°; after (c) 2k impacts and (d) 10k impacts at 80°; for 1000 eV Ar^+ after (e) 2k impacts and (f) 4k impacts at 70°; and after (g) 2k impacts and (h) 4k impacts at 80°. Only atoms deviating from the initial FCC structure are plotted.

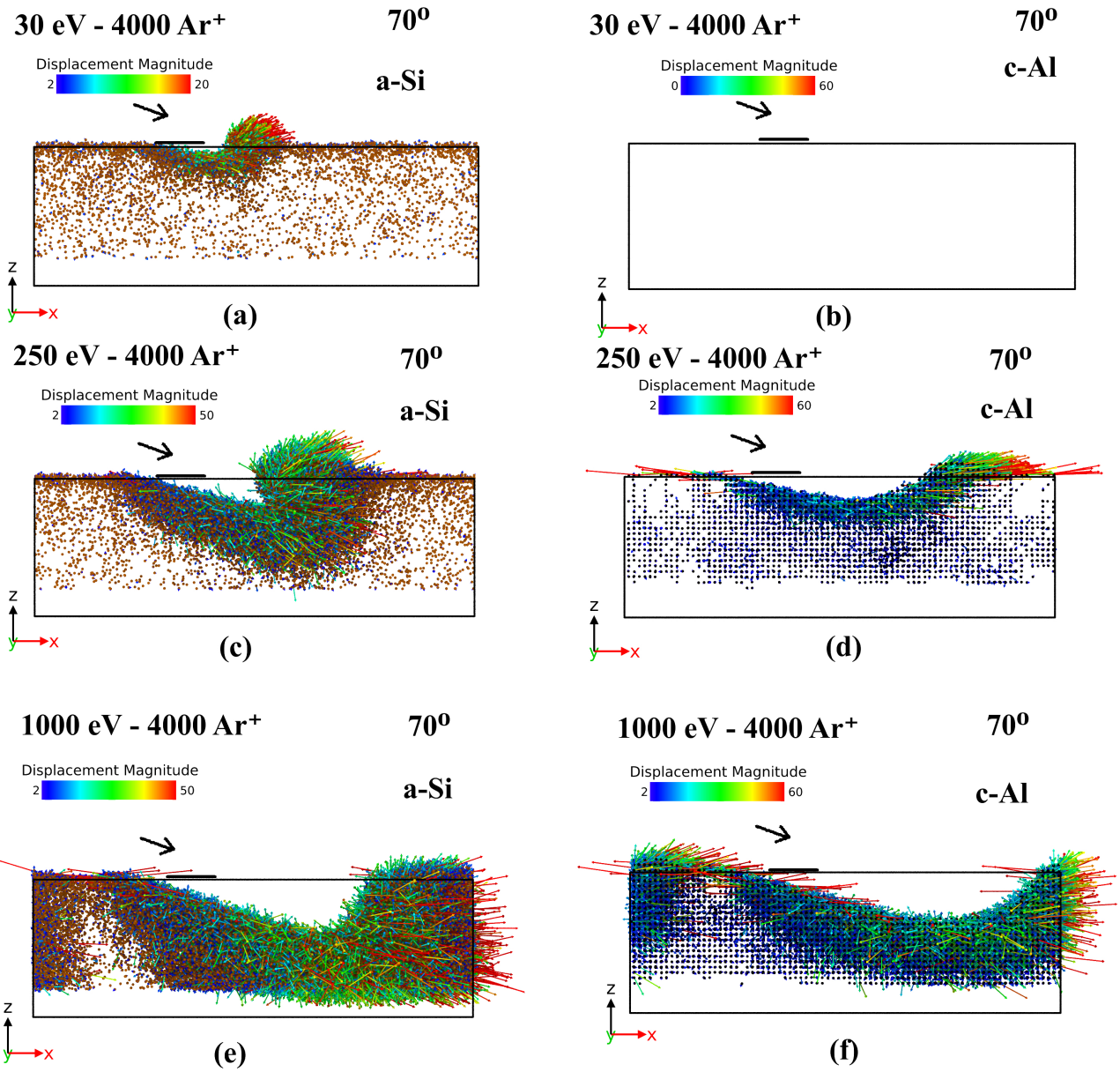

FIG. 11: a-Si cell after 4000 Ar^+ at 70° for (a) 30 eV (from Ref. 13), (c) 250 eV and (e) 1000 eV (in FIG. 4b); c-Al cell after 4000 Ar^+ at 70° for (b) 30 eV, (d) 250 eV and (f) 1000 eV (in FIG. 7b). Only displacements greater than 2 Å are presented and the displacement vectors are scaled by a factor of 0.3 for a better visualization; in the case of 30 eV Ar^+ on c-Al the initial structure has not been damaged during irradiation (no atom is either displaced more than the thermal vibration or sputtered). The initial impact region is marked in black.

fluence (FIG. 11b). On the other hand, in a-Si the low energy patterning effect is quite clear, which was also proven experimentally[13].

We also analyse the pattern formation in terms of the volume of the formed groove and the ridge by finding the total volume of sputtered atoms ($N_{\mathrm{sputt}} \cdot V_{\mathrm{atom}}$) and the volume built up by the adatoms ($N_{\mathrm{adatoms}} \cdot V_{\mathrm{atom}}$). The former are the atoms which are sputtered away from the surface, and the latter are those which remained in the system but were displaced above the initial surface level during the irradiation. The volumes considered for the analysis are 0.02 nm^3 and 0.017 nm^3 for Si and Al, respectively. In the FIG. 12 we observe that the largest groove is built by Ar ions with the energy of 1000 eV, however, the size of the groove in c-Al is larger than in a-Si (the average sputtering yields of Si and Al in our simulations deduced from the respective figures are ~ 2.2 (FIG. 5a) and ~ 3.5 (FIG. 8a), respectively).

The most prominent growth of a ridge we observe for the Ar ion energy of 250 eV, for the ions of 1000 eV, the ridge also grows quite rapidly at the beginning, however, the growth slows down after 2000 – 2500 impacts. The growth of a ridge is practically not observed for the c-Al cell.

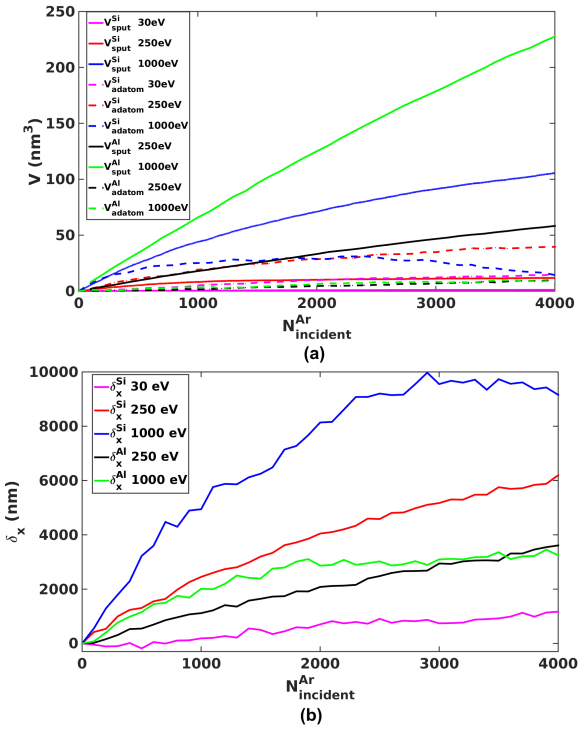

FIG. 12: Evolution of (a) the volume created by the sputtered atoms and adatoms and (b) the accumulated displacement in the x direction for 30 eV (from Ref. 13), 250 eV and 1000 eV Ar$^+$ for a-Si and for 250 and 1000 eV Ar$^+$ for c-Al at 70°.

In FIG. 12, we compare how the magnitude of the x component of the total displacement (δ_x) and the erosion mechanism depend on the material and irradiation energy. In the case of a-Si, most of the displacements are small, the total displacement accumulates slowly as can be seen in FIG. 12b. While comparing δ_x for c-Al and a-Si, we see that in spite of the longer displacements due to the discreteness of these displacements, the total number of them is smaller in c-Al compared to the corresponding energy case for a-Si; the x component of the total displacement is considerably higher for the latter material than for the former one. The evolution of the total displacement for 250 eV and 1000 eV is very similar for c-Al at 70°, although the groove formed in these simulations was different. This result underlines the importance of the erosion mechanism in the ripple formation in the crystalline material, which is much less obvious for the amorphous case. The measure of the sputtering contribution compared to the total volume of the cell is qualitatively intuitive.

Since in FIG. 12a we show only the volume, which was taken away by the sputtered atoms, next we analyze the total loss of volume in the irradiated samples. In TABLE I we present the comparison of the volume loss estimated as in as FIG. 11a and as the difference between the volume of the initial cell and the volume occupied by the atoms bound in the structure at a given fluence. For the latter, we used the surface mesh construction algorithm implemented in OVITO[37], which allows to calculate the actual (solid) volume of the cell. The difference between the original volume and the solid volume calculate within the contour outlining the surface of the simulation cell after the 4000 ion impacts, we obtain the volume loss, in other words, the volume occupied by the groove of the forming ripple. If there were no effect of redistributive mechanism in these simulations, the following equality must hold:

$$V_{groove} = V_{orig} - V_{solid} \text{ (if no redistribution)} \qquad (2)$$

In the EQ. (2) the V_{groove} represents the volume occupied by the groove, which is the difference between the initial volume of the cell (V_{orig}) and the solid volume of the cell after 4000 Ar$^+$ impacts (V_{solid}). The V_{groove} should match also:

$$V_{groove} = V_{sput} - V_{adatom} + V_{Ar} + V_{redist} \qquad (3)$$

The left part of the EQ. (3) is shown in the second column of TABLE I and called V_{groove}, while V_{sput} (volume sputtered away) and V_{adatom} (volume over the initial surface level) are given in the 4th and 5th columns, respectively. On the other hand, if there would be no redistribution by small displacements ($V_{\mathrm{redist}} = 0$), ripple formation is only driven by sputtering, then one should have $V_{\mathrm{no-redistribution}} = V_{\mathrm{sput}} - V_{\mathrm{adatom}} + V_{\mathrm{Ar}}$ ($V_{\mathrm{no-redistribution}}$ shown in the 3rd column). We do not analyze the extra volume added by of Ar atoms (V_{Ar}) as even the largest

concentration of these atoms implanted into the simulation cell did not exceed 1 %.

TABLE I: Volume loss induced by irradiation in a-Si and c-Al targets after 4000 Ar^+ impacts at 30 eV[13], 250 eV and 1000 eV. The units are nm^3.

	V_{groove}	$V_{no-redistribution}$	V_{sput}	V_{adatom}
30 eV Ar^+ - a-Si	54.93	-13.74	1.09	14.83
250 eV Ar^+ - a-Si	67.21	-27.82	11.76	39.58
1000 eV Ar^+ - a-Si	241.3	91.17	105.56	14.39
250 eV Ar^+ - c-Al	113.58	48.49	58.27	9.78
1000 eV Ar^+ - c-Al	281.12	218.44	227.58	9.14

Analyzing the data presented in TABLE I we can measure the difference in the pattern formation in the studied range of energies and both studied materials. Practically in all the cases for a-Si the equality 2 does not hold. The empty volume created after the irradiation cannot be explained only by the non-redistributive effects ($V_{\mathrm{no-redistribution}}$). Only in the case of the highest energy of irradiation it reaches about a 38% of the total volume created (V_{groove}), showing that the redistributive mechanism (62%) due to atomic displacements during irradiation is the leading force of the ripple formation. This fact was proved for 30 eV Ar^+ in Ref. 13. We can find that erosion in general is taking a more determinant role as the energy of incident ion is increasing, which means that the pattern formation could be driven by erosion in an amorphous sample if the energy is high enough. On the other hand, the formation of any structure at low or ultra-low energies is unlikely due to erosion, as can be seen in TABLE I and in Ref. 13. In the 1000 eV case, we see that the volume created differs considerably of the sum of the V_{sput} and V_{adatom}. The reason is because the momentum induced by the ion the material makes the atoms move partially downward, at some point they are removed when the atoms get stuck in the fixed layer. So that contribution can be counted as a part of the redistributive contribution, which means that even at high energies, in a-Si the redistribution mechanism is the main reason of pattern formation.

The discussion on the formation in c-Al points to other direction. We can see that the erosive mechanism is more prominent in the ripple formation on crystal surfaces as the non-redistributive volume is about 43% of the estimated volume loss for the 250 eV irradiation and about the 78% for the 1000 eV case $V_{\mathrm{no-redistribution}}$. Thus we conclude that the sputtering is more important in pattern formation on the surface of a c-Al structure (see FIG. 8 a) than in a-Si (see FIG. 5 a). It is possible to observe patterns on c-Al, nevertheless they have been reported at higher energies (16.7 keV Ar^+ (Ref. 23) and O_2^+ (Ref. 22)). As is described in Ref. 22, the erosion is the driving mechanism of the pattern formation and, even though we are simulating a "single-ripple" case, we can get similar conclusions out of our results, showing that the erosion mechanism could be the dominant explanation to the surface modification in crystalline materials such as c-Al. Since V_{sput} is the main part in all the c-Al cases, the erosion is the reason of the creation and it is strengthened by the fact that at 30 eV irradiation nothing changes, establishing that no erosion means no surface modification in the Al case. The crystalline structure of the metal only allows the atoms be displaced a discretely distributed distance (see FIG. 10) or leave the system. The redeposition of atoms under certain circumstances could contribute to the formation[22], but that mechanism is not discussed here.

In the light of the presented results, we can see that, using this "single-ripple" formation model, the explanation of the formation of patterns in surface is not only dependent on the energy and angle, but on the structure of the irradiated material. Comparing the results for V_{groove} and $V_{\mathrm{no-redistribution}}$, we can clearly see that the redistributive mechanism is having more importance in the a-Si structure in general than in the c-Al. The sputtering is dominant in the c-Al structure and the erosion takes more weight at higher irradiation energies.

IV. CONCLUSION

We have performed sequential irradiation simulations for a-Si and c-Al targets for the low and medium ion energies: 30 eV, 250 eV and 1 keV Ar^+ ions. The method to perform such simulations has already been utilized by us in a low energy irradiation setup[13]; now we have applied it successfully for higher energies and with a crystalline material. We have compared how the different materials behave under similar conditions and observed that in the case of a-Si is easier to displace atoms within the cell (redistribution) but is harder to sputter atoms away (erosion) due to the formation of the ridge where the initially sputtered atoms redeposit for 70°, since the change of the impact region is quite prominent. On the other hand in c-Al, the erosion is higher than in a-Si but at the same time the redistribution is smaller. The formation of a groove is also possible in c-Al, showing that defect creation is needed to observe a modification of the surface.

Based in the volume analysis, we can see that the higher the energy is, the effect of erosion is taking more importance in the groove formation. On the other hand, for lower energies, the groove is generally formed as a product of accumulated atomic displacements.

The structure of the material turned out to be a crucial topic in the pattern formation. The model developed in this work alongside the volume analysis, showed that the formation in c-Al is not due to the same reasons as in a-Si. In the range of energies presented here, the redistribution mechanism is the reason of the pattern formation in amorphous materials due to mostly small displacements, while in the crystalline, the relative importance of this mechanism is diminished by the erosion, which is the

driving force in the formation of the ripple.

ACKOWLEDGEMENTS

The work was performed within the Finnish Centre of Excellence in Computational Molecular Science (CMS), financed by The Academy of Finland and University of Helsinki. Computational resources provided by CSC, the Finnish IT Center for Science as well as the Finnish Grid and Cloud Infrastructure (persistent identifier urn:nbn:fi:research-infras-2016072533) are gratefully acknowledged.

* Corresponding author alvaro.lopezcazalilla@helsinki.fi

[1] D. Chowdhury, D. Ghose, and S. A. Mollick, Vac. **107**, 23 (2014).
[2] D. Chowdhury, D. Ghose, S. A. Mollick, B. Satpati, and S. R. Bhattacharyya, Phys. Status Solidi B **252**, 811 (2015).
[3] B. Ziberi, F. Frost, T. Höche, and B. Rauschenbach, Phys. Rev. B **72**, 235310 (2005).
[4] C. S. Madi, B. D. nad H. Bola George, S. A. Norris, M. P. Brenner, and M. J. Aziz, Phys. Rev. Lett. **101**, 246102 (2008).
[5] C. S. Madi, B. D. nad H. Bola George, S. A. Norris, M. P. Brenner, and M. J. Aziz, Phys. Rev. Lett. **107**, 049902 (2011).
[6] C. S. Madi, H. B. George, and M. J. Aziz, J. Phys. Condes. Matt. **21**, 224010 (2009).
[7] C. S. Madi, E. Anzenberg, K. F. L. Jr., and M. J. Aziz, Phys. Rev. Let. **106**, 066101 (2011).
[8] W. L. Chan and E. Chason, J. Appl. Phys. **121301**, 46 (2007).
[9] J. Muñoz-García, L. Vázquez, R. Cuerno, J. Sánchez-Garcí́a, M. Castro, and R. Gago, edited by Z. M. Wang, Springer, Dordrecht **10**, 323 (2009).
[10] A. Lopez-Cazalilla, A. Ilinov, L. Bukonte, F. Djurabekova, K. Nordlund, S. Norris, and J. Perkinson, Nucl. Instr. Meth. Phys. Res. B **414**, 133 (2018).
[11] S. A. Norris, J. Samela, C. S. Madi, M. P. Brenner, L. Bukonte, M. Backman, F. Djurabekova, K. Nordlund, and M. J. Aziz, Nature communications **2**, 276 (2011).
[12] S. A. Norris, M. P. Brenner, and M. J. Aziz, Journal of Physics-Condensed Matter **21**, 224017 (2009).
[13] A. Lopez-Cazalilla, A. Ilinov, K. Nordlund, D. Chowdhury, S. R. Bhattacharyya, D. Ghose, S. Mondal, P. Barman, F. Djurabekova, and S. Norris, J. Appl. Phys. **123**, 235108 (2018).
[14] P. Sigmund, Phys. Rev. **184**, 383 (1969).
[15] R. M. Bradley and J. M. Harper, J. Vac. Sci. Technol. **6**, 2390–2395 (1988).
[16] M. Harrison and R. Bradley, Phys. Rev. B **89**, 245401 (2014).
[17] H. Hofsäss, Appl. Phys. A **114**, 401 (2014).
[18] H. Hofsäss, K. Zhang, H. G. Gehrke, and C. Brüsewitz, Phys. Rev. B **88**, 075426 (2013).
[19] L. Bukonte, F. Djurabekova, J. Samela, K. Nordlund, S. A. Norris, and M. J. Aziz, Nucl. Instr. Meth. Phys. Res. B **297**, 23 (2013).
[20] K. Nordlund, S. Zinkle, A. Sand, F. Granberg, R. Averback, R. Stoller, T. Suzudo, L. Malerba, F. Banhart, J. Weber, F. Willaime, S. Dudarev, and D. Simeone, Nature communications **9**, 1084 (2018).
[21] P. Karmakar and D. Ghose, Surf. Sci. **554**, L101 (2004).
[22] P. Mishra and D. Ghose, Phys. Rev. B **74**, 155427 (2006).
[23] P. Mishra and D. Ghose, J. Appl. Phys. **104**, 094305 (2008).
[24] D. Ghose, J. of Phys.: Condensed Matter **21**, 22 (2009).
[25] U. Valbusa, C. Boragno, and F. Buatier de Mongeot, J. Phys.: Condens. Matter **14**, 8153 (2002).
[26] M. Ghaly, K. Nordlund, and R. S. Averback, Phil. Mag. A **79**, 795 (1999).
[27] K. Nordlund, M. Ghaly, R. S. Averback, M. Caturla, T. D. de la Rubia, and J. Tarus, Phys. Rev. B **57**, 7556 (1998).
[28] Y. Yamamura, Y. Itikawa, and N. Itoh, *Angular dependence of sputtering yields of monatomic solids*, Report IPPJ-AM-26 (Institute of Plasma Physics, Nagoya University, 1983).
[29] J. Fluit, P. Roi, and J. Kistemaker, J. Appl. Phys. **34**, 690 (1963).
[30] K. Nordlund, Comput. Mater. Sci. **3**, 448 (1995).
[31] F. Ercolessi and J. B. Adams, Europhys. Lett. **26**, 583 (1994).
[32] J. F. Ziegler, J. P. Biersack, and U. Littmark, (Pergamon, New York) (1985).
[33] K. Nordlund, M. Ghaly, and R. S. Averback, J. Appl. Phys. **83**, 1238 (1998).
[34] K. Nordlund, N. Runeberg, and D. Sundholm, Nucl. Instr. Meth. Phys. Res. B **132**, 45 (1997).
[35] C. Kittel, *Introduction to Solid State Physics*, 3rd ed. (John Wiley & Sons, New York, 1968).
[36] J. Nord, K. Nordlund, and J. Keinonen, Phys. Rev. B **65**, 165329 (2002).
[37] A. Stukowski, JOM **66**, 399 (2014).